Hybrid Advances 10 (2025) 100429

Contents lists available at ScienceDirect

Hybrid Advances

journal homepage: www.journals.elsevier.com/hybrid-advances

Research Article

Advancement in tribological performance of hexagonal Bi_2Te_3 nanosheets by incorporation of Ag_2MoO_4 nanoparticles

Somesh Singh [a], Muskan Sahu [a], Satypal Prajapati [a], Anup Kumar [b], Murli Dhar Mitra [c], Aditya Kumar [c], Dhanesh Tiwary [b], Dinesh K. Verma [a,*]

[a] Department of Chemistry, Prof. Rajendra Singh (Rajju Bhaiya) Institute of Physical Sciences for Study & Research, V.B.S. Purvanchal University, Jaunpur, 222003, India

[b] Department of Chemistry, Indian Institute of Technology (Banaras Hindu University), Varanasi, U.P, 221005, India

[c] Department of Chemical Engineering, Indian Institute of Technology (Indian School of Mines), Dhanbad, Jharkhand, 826001, India

ARTICLE INFO

Keywords:
Bi_2Te_3 nanosheets
Ag_2MoO_4 nanoparticles
Nanocomposites
Surface characterization
Tribological properties

ABSTRACT

The hydrothermal, and co-precipitation methods were used to synthesize bismuth telluride (Bi_2Te_3) nanosheets, and silver molybdate (Ag_2MoO_4) nanoparticles, respectively to improve the tribological activity of lubricating oil. Being a hexagonal 2D structure, Bi_2Te_3 nanosheets are considered to be tribologically active. With a purpose to have the tribological activity of high order, an attempt has been made to decorate Bi_2Te_3 nanosheets with Ag_2MoO_4 nanoparticles in the form of nanocomposite Ag_2MoO_4/Bi_2Te_3. The morphological analysis of Ag_2MoO_4/Bi_2Te_3 nanocomposites using HR-SEM, TEM, and HR-TEM, confirms a uniform distribution of nanoparticles throughout the Bi_2Te_3 nanosheets. The tribological efficacy of the extensively analyzed nanomaterials was assessed in base lube (paraffin oil) at an optimized concentration, 0.03 % w/v, employing a four-ball tester executing ASTM D4172 and ASTM D5183 tests. Based on the analyzed tribological data, mean wear scar diameter (MWD), coefficient of friction (COF), and seizure load, synthesized nano additives exhibited superior tribological performance compared to the base oil. The antiwear and antifriction efficiency was found in the following order- $Ag_2MoO_4/Bi_2Te_3 \gg Ag_2MoO_4 > Bi_2Te_3$, and $Ag_2MoO_4/Bi_2Te_3 \gg Bi_2Te_3 > Ag_2MoO_4$, respectively.

The nanocomposites demonstrated significantly enhanced tribological activity attributable to the synergistic interaction between noncovalently bonded nanosheets and nanoparticles. All constituent elements, elemental composition, and metal oxides (Bi_2O_3, TeO_2, Ag_2O, MoO_3, MoO_2, and Fe_2O_3) formed in the tribofilm, have collectively contributed to the lubrication, were validated through energy-dispersive X-ray spectroscopy (EDX) and XPS techniques. The SEM and AFM investigations of the lubricated surface verified the result of antiwear and antifriction.

1. Introduction

The field of tribology deals with the investigation of friction, wear, and lubrication, which plays a key role in ensuring the effective operation of various mechanical components such as bearings, piston rings, and gears. Moreover, aside from its applications in engineering, tribology also extends its reach to various aspects of our everyday lives, including contact lenses and cosmetics. The direct association of tribology with energy and fuel efficiency further emphasizes its significance in light of global challenges, such as the depletion of finite natural resources like fossil fuels and minerals and the continuous rise in CO_2 emissions leading to global warming [1]. In the current situation, it has been recognized that friction and wear significantly contribute to a decrease in energy efficiency, thereby prompting the exploration and development of more environmentally friendly lubricants [1,2].

The nanoparticles made by nontoxic elements, generally do not impose any adverse effect on the environment compared to traditional lubricant additives [2]. It is well documented in various research articles that the blends of nanoparticles lead to a reduction in friction and wear by serving as load-bearing material, and tribosinterization [3–6]. Various lubrication mechanisms, such as the mending, the rolling, and the polishing effect through the formation of a protective film, have

* Corresponding author.
E-mail address: dineshkv.rs.chy15@iitbhu.ac.in (D.K. Verma).

https://doi.org/10.1016/j.hybadv.2025.100429
Received 23 December 2024; Received in revised form 21 February 2025; Accepted 4 March 2025
Available online 7 March 2025

been suggested to elucidate the function of nanoparticles in lubricating oil [3,7,8]. Lots of metal, metal oxide, and binary metal oxides are used as lubricant additives under different tribo-conditions [6,9–11]. The binary metal oxides are well known for their environmental adaptability as nano additives and have good tribological performance at high temperatures. Examples of such oxides include; AgMoxOy, AgVxOy, and CaWxOy, which have been shown to possess low friction coefficients ranging from 0.2 to 0.4 at temperatures above 500 °C [12,13]. Hao et al. (2021) investigated that during the NiCoCrAlYTa/Ag/Mo composite coating when the temperature increases up to 600 °C, the external diffusion and oxidation processes of both silver (Ag) and molybdenum (Mo) contribute to the in situ creation of Ag_2MoO_4 on the surface of the coating. The stratified nature of Ag_2MoO_4 allows for the development of a consistent lubricating film at 800 °C, consequently enhancing the ability of the composite coating to exhibit superior tribological characteristics [14]. Yang et al. (2021) reported synergistic lubrication through the incorporation of Ag and Ag_2MoO_4 nanoparticles within plasma-sprayed YSZ coatings at 800 °C [13].

Two-dimensional (2D) nanomaterials like graphene, transition metal dichalcogenides (TMDs), and hexagonal boron nitride (h-BN) have experienced a significant surge in popularity owing to their properties and applicability in domains such as sensors, catalysis, optoelectronics, electronics, energy storage devices like- Li-ion batteries, solar cells, and reinforced ceramics, as well as biomedical and tribological applications [15–17]. In conjunction with nanoparticles, numerous 2D layered materials including tungsten disulfide (WS_2), hexagonal boron nitride (h-BN), molybdenum disulfide (MoS_2), and graphene-based materials, are also utilized multiple times as lubricant additives. These materials exhibit distinctive structures with a remarkable specific surface area, robust in-plane rigidity, and feeble interlayer interaction [18–21].

In the midst of inorganic nanomaterials, chalcogenides of bismuth (Bi_2X_3, X = O, S, Se, and Te) are cost-effective and have controllable shape and size, high stability, narrow bandgap, high ionic conductivity, and environmentally sustainable properties [22,23]. The frictional properties of mixtures containing bismuth sulfide (Bi_2S_3) in vinyl-terminated silicone fluid (PDMS-Vi) were investigated through block-on-ring tests (polymer/steel) and Reichert's test on steel-steel tribo-system [24]. The formation of in situ Bi_2S_3 was observed during the tribological test of bismuth carboxylate-polysulfide combinations as additives in extreme-pressure conditions [25]. The tribological studies of Bi_2S_3 as a solid lubricant [26] at a temperature of 580 °C, and Bi_2S_3 soft coatings [27] were assessed through reciprocating sliding tests. Nivedita et al. (2023) investigated the antifriction and antiwear properties of Bi_2Se_3 nanosheets used as additives in paraffin base lube [28]. The Bi_2Te_3 is extensively utilized in a wide range of applications such as photocatalysts [29], thermoelectric materials [30,31], dielectric [32], photodetectors [33,34], electrochemical sensors [35], supercapacitors [36], and recently in biomedical fields [37,38]. but no studies were reported in the field of tribology. Since Bi_2S_3 and Bi_2Se_3 are tribologically active and Bi_2Te_3 belongs to the same family with analogous characteristics in various domains, it is anticipated that Bi_2Te_3 may exhibit good tribological properties.

The nanoparticles (NPs) and nanosheets (NSs) show the phenomena of agglomeration and restacking, respectively, making it hard to disperse in the base oil [11,39,40]. To address this issue, numerous researchers have successfully demonstrated that the formation of nanocomposites can reduce its aggregation and restacking and enhance the dispersion in base oil [10,41–43]. The preparation of nanocomposites also enhances the tribological properties by leveraging the synergistic effects of nanosheets and nanoparticles [13,44,45]. Our research group synthesized nanocomposites of Bi_2Se_3/Bi_2WO_6 and Bi_2Se_3/N-Doped Bi_2WO_6 and investigated the tribological properties as additives in the paraffin base oil and found increased lubrication efficiency compared to its individual components [28].

This investigation explored the tribological characteristics of Ag_2MoO_4 nanoparticles as well as Bi_2Te_3 nanosheets, along with their nanocomposites (Ag_2MoO_4/Bi_2Te_3) in paraffin base lube. The tribological properties of the various synthesized additives at different concentrations were analyzed using a four-ball wear test machine. The worn surfaces lubricated with different nano additives were analyzed using atomic force microscopy (AFM) and scanning electron microscopy (SEM). The elemental composition of the tribofilm formed on the lubricated surface with Ag_2MoO_4/Bi_2Te_3 nanocomposites was determined using X-ray photoelectron spectroscopy (XPS) and energy-dispersive X-ray spectroscopy (EDX).

2. Experimental section

2.1. Materials

All the chemicals utilized in this research work are analytical grade and used directly. $Na_2MoO_4.2H_2O$, Bi_2O_3, PVP, and $NaBH_4$ were purchased from CDH, whereas TeO_2 and $AgNO_3$ were procured from TCI and qualigens, respectively.

2.2. Synthesis of nano additives

2.2.1. Synthesis of Bi_2Te_3 nanosheets

The Bi_2Te_3 nanosheets were synthesized using a previously reported methodology [32]. For synthesizing Bi_2Te_3 nanosheets, 0.466 g Bi_2O_3, 0.4788 g TeO_2, 0.64 g NaOH, and 1.7 g PVP were used as precursors. Firstly, 36 ml ethylene glycol was used to dissolve 1.7 g of PVP with the help of sonication. After that, in the prepared PVP solution, both Bi_2O_3 and TeO_2 were dissolved completely by vigorous stirring. Later on, NaOH dissolved in 4 mL DI water was mixed in the prepared solution and stirred for 40 min to obtain a uniform solution. Further, the reaction mixture was transferred to a 100 ml Teflon-lined autoclave and heated in a hot air oven at 200 °C for 4.5 h. When the autoclave was cooled down to room temperature (R.T.), the synthesized nanosheets were washed with moderate acetone solution several times and dried at 60 °C for 6 h to obtain black-colored Bi_2Te_3 nanosheets.

2.2.2. Synthesis of Ag_2MoO_4 nanoparticles

The aforementioned co-precipitation method was utilized to synthesize Ag_2MoO_4 NPs without adding surfactant [46]. Initially, the solution of $Na_2MoO_4.2H_2O$ (1 mM) and $AgNO_3$ (2 mM) was prepared with 10 ml DI water by stirring for 30 min. Thereafter, the solution of $Na_2MoO_4.2H_2O$ was poured dropwise in the $AgNO_3$ solution and stirred vigorously at R.T. for 60 min. The resulting sediment was washed repeatedly using DI water and centrifuged to remove any impurities. To obtain the Ag_2MoO_4 NPs, the precipitate was dried in a vacuum oven at 60 °C up to 24 h.

2.2.3. Synthesis of Ag_2MoO_4/Bi_2Te_3 nanocomposites

A similar method was utilized for fabricating the nanocomposites as described previously [47]. The (0.6 g) synthesized Bi_2Te_3 NSs dispersed in the mixture of water and ethanol (1:1 ratio) using ultra-sonication for 2 h. After that, (1.18 g) of $AgNO_3$ was added while continuing sonication. After the sonication process, the prepared solution of $Na_2MoO_4.2H_2O$ (0.84g $Na_2MoO_4.2H_2O$ in 35 ml DI water) was poured dropwise in the prior solution and stirred continuously for 2 h. The obtained mixture was then washed with ethanol and water consecutively before being dried in the oven at 80 °C for 24 h. The schematic presentation for the synthesis of the Ag_2MoO_4/Bi_2Te_3 nanocomposites is presented in Scheme 1.

3. Result and discussion

3.1. Morphology and microstructure of the synthesized nano additives

The prepared nano additives; Bi_2Te_3 NSs, Ag_2MoO_4 NPs, and Ag_2MoO_4/Bi_2Te_3 nanocomposites were characterized using various

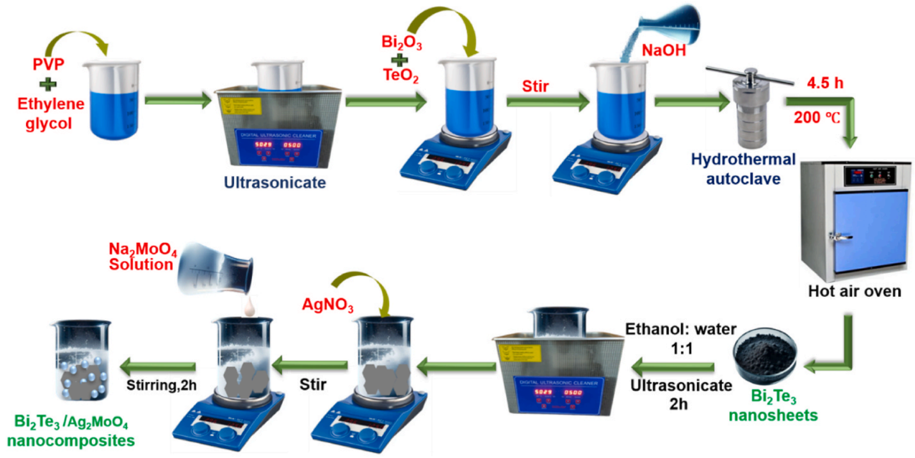

Scheme 1. Schematic presentation for the synthesis of $\mathbf{Ag_2MoO_4/Bi_2Te_3}$ **nanocomposites**.

state-of-the-art techniques, like p-XRD, HR-SEM, UV/visible, FT-IR, and TEM/HR-TEM. Additionally, XPS has been used to characterize the chemical composition of Ag_2MoO_4/Bi_2Te_3 nanocomposites.

Fig. 1a displays the X-ray diffraction analysis of the synthesized nano additives; Ag_2MoO_4, Bi_2Te_3, and Bi_2Te_3/Ag_2MoO_4. As demonstrated by Fig. 1a, the diffraction peaks of Ag_2MoO_4 NPs observed at 16.39°, 27.07°, 31.81°, 33.33°, 38.80°, 42.39°, 47.86°, 50.03°, 55.92°, 58.80°, 63.35°, 65.82°, 66.70°, 70.25°, 76.76°, and 79.05°, which can be indexed as (111), (220), (311), (222), (400), (331), (422), (511), (440), (531), (620), (533), (622), (444), (642) and (731), planes respectively. The sharp XRD peaks confirmed the purity and crystallinity of Ag_2MoO_4 NPs having a spinel, cubic structure matched with JCPDS card No-08-0473 [46]. The XRD pattern of Bi_2Te_3 shows diffraction peaks at 17.58°, 23.70°, 27.90°, 38.12°, 41.52°, 45.02°, 50.50°, 54.09°, 57.03°, 62.39°, 66.08°, 67.08°, 70.50°, 72.98°, and 75.16° corresponding to (006), (101), (015), $(10\underline{10})$, $(10\underline{11})$, (110), $(00\underline{15})$, (013), (205), $(10\underline{16})$, $(02\underline{10})$, $(11\underline{15})$, $(01\underline{20})$, (125), and $(21\underline{10})$ planes (JCPDS card No-15-0863) [6]. Almost all the peaks of constituents nanomaterials were present in the XRD of Ag_2MoO_4/Bi_2Te_3 nanocomposites confirming the successful synthesis of nanocomposites.

The FT-IR spectra of Bi_2Te_3, Ag_2MoO_4, and Bi_2Te_3/Ag_2MoO_4 are shown in Fig. 1b. A clear peak at 823 cm^{-1} in the FT-IR spectra of Ag_2MoO_4 nanoparticles demonstrates, the anti-symmetric stretching vibrations of the O–Mo–O bond. Moreover, a notable peak at around 1642 cm^{-1} along with a broad peak within the 3200-3400 cm^{-1} range, corresponds to the bending and stretching vibrational modes of the hydroxyl group of water molecules (due to the atmospheric moisture), respectively [48]. The FT-IR spectrum of bismuth telluride (Bi_2Te_3) demonstrates a broad subtle absorption peak at approximately 3290 cm^{-1}, which can be attributed to the presence of the hydroxyl (-OH) group due to moisture. Another low intense peak, falling around 1010 and 1592 cm^{-1}, is indicative of a C–H bond, and the carbon-oxygen (C═O) bond, respectively. A strong peak around 638 cm^{-1} is attributed to the Bi–O bond within the material [49]. The FT-IR spectrum of Bi_2Te_3/Ag_2MoO_4 nanocomposites shows the presence of almost all the peaks of constituent materials with slight shifting validating the synthesis of nanocomposites.

The HR-SEM images of Ag_2MoO_4, Bi_2Te_3, and Ag_2MoO_4/Bi_2Te_3 have been recorded to analyze the morphological and microstructural features, as shown in Fig. 2 (a,b & d). HR-SEM image of Ag_2MoO_4 showed spherical nanoparticles as evident in Fig. 2a and on the other hand, a 2D-hexagonal layered structure with approximately 500 nm width, and

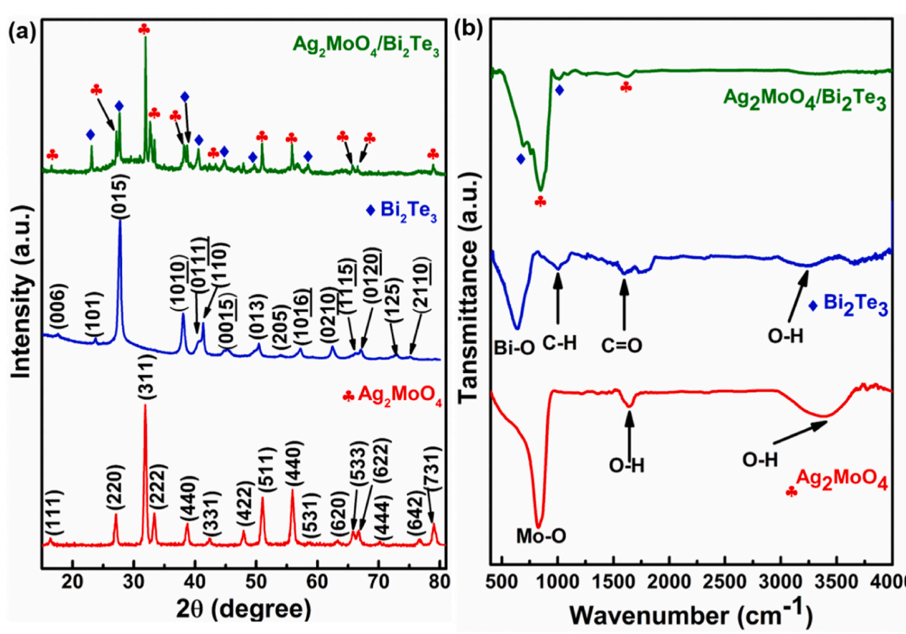

Fig. 1. (a) XRD patterns and (b) FT-IR spectra of Ag_2MoO_4, Bi_2Te_3, and Bi_2Te_3/Ag_2MoO_4.

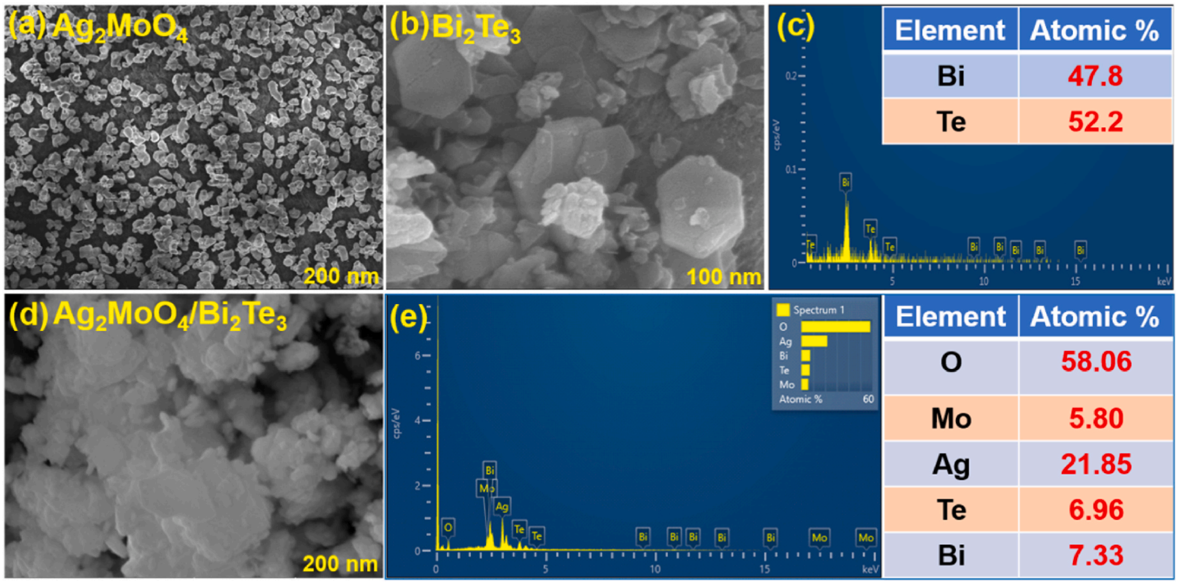

Fig. 2. HR-SEM images of (a) Ag_2MoO_4 (b) Bi_2Te_3 (c) EDX of Bi_2Te_3 (d) HR-SEM image, and (e) EDX-spectra of Ag_2MoO_4/Bi_2Te_3 nanocomposites.

10–15 nm thickness of Bi_2Te_3 NSs was confirmed in Fig. 2b [32]. The EDX spectrum of Bi_2Te_3 nanosheets is displayed in Fig. 2c. The tribological performances are affected by the thickness and size of NSs, the thinner the nanosheets, the better they penetrate the sliding interfaces [11]. The HR-SEM image of the Ag_2MoO_4/Bi_2Te_3 nanocomposite (Fig. 2d) synthesized via in situ co-precipitation, shows nanoparticles grown on Bi_2Te_3 nanosheets. This confirms the successful formation of the nanocomposites, as both nanoparticles and nanosheets are clearly visible. EDX analysis of prepared Ag_2MoO_4/Bi_2Te_3 demonstrated that all elements such as Ag, Mo, O, Bi, and Te are present in the prepared nanocomposites as shown in Fig. 2e. The elemental mapping of prepared Ag_2MoO_4/Bi_2Te_3 nanocomposites is displayed in Fig. S1 (Supplementary Materials File).

TEM images of the synthesized nanoadditives have also been captured to analyze the refined morphology, as illustrated in Fig. 3(a–c) and HR-TEM Fig. 3 (a_1-c_1). The spherical shape of nanoparticles is evident in the TEM image of Ag_2MoO_4 as displayed in Fig. 3a and has an average particle size of around 12 nm as shown in the inset of Fig. 3a. An analysis of the HR-TEM image of Ag_2MoO_4 nanoparticles is displayed in Fig. 3a_1, which showed uniform lattice fringes having a d-spacing of

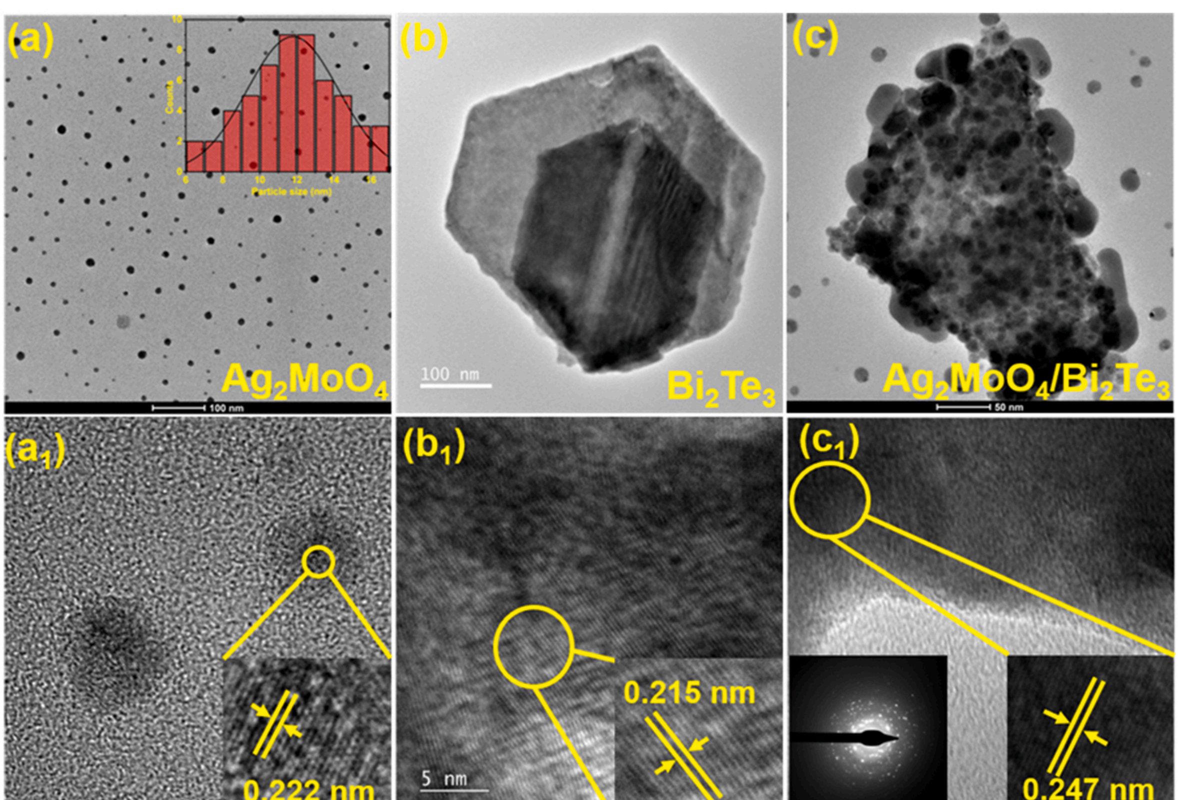

Fig. 3. TEM images of (a) Ag_2MoO_4 (b) Bi_2Te_3 (c) Ag_2MoO_4/Bi_2Te_3 and HR-TEM image of (a_1) Ag_2MoO_4 (b_1) Bi_2Te_3 (c_1) Ag_2MoO_4/Bi_2Te_3.

0.222 nm, closely corresponds to (400) planes, as documented in the JCPDS card number 08–0473 [50].

Furthermore, the TEM image confirms a hexagonal layered structure of Bi_2Te_3 NSs as shown in Fig. 3b. Investigation of the HR-TEM image of Bi_2Te_3 (Fig. 3b$_1$), displays structurally uniform lattice fringes spaced at 0.215 nm corresponding to the $(11\ \overline{20})$ planes in compliance with the previous reports [31,32]. The Ag_2MoO_4 nanoparticle anchored onto the Bi_2Te_3 nanosheets in the Ag_2MoO_4/Bi_2Te_3 nanocomposites is illustrated in Fig. 3c. The HR-TEM images of the Ag_2MoO_4/Bi_2Te_3 nanocomposites indicate that the interlayer spacing of the Bi_2Te_3 related to the $(11\overline{2}0)$ plane has slightly increased from 0.215 nm to 0.247 nm, (Fig. 3c$_1$). The augmentation in the distance within layers of the $(11\overline{2}0)$ plane of Bi_2Te_3 NSs suggests that nanosheets have effectively interacted with Ag_2MoO_4 NPs in nanocomposite formation [28,51]. The polycrystalline characteristics of the prepared nano additives were demonstrated by the selected area electron diffraction (SAED) patterns, as shown in the inset of Fig. 3(c$_1$).

The chemical states of the elements present in the Ag_2MoO_4/Bi_2Te_3 nanocomposites have been examined using X-ray photoelectron spectroscopy (XPS). With the help of peak fir software, Fig. 4(a–e) represents the core-level spectra of Bi 4f, Te 3d, Ag 3d, Mo 3d, and, O 1s respectively. Specifically, the XPS peaks of Bi 4f were observed at 157.07 and 162.44 eV, as shown in Fig. 4a, demonstrating good alignment with the binding energies of $4f_{7/2}$ and $4f_{5/2}$, respectively, confirming the presence of Bi^{+3} in Bi_2Te_3 [28,52]. In addition, the appearance of Te 3d peaks at 574.99 and 585.44 eV related to Te $3d_{5/2}$ and Te $3d_{3/2}$, respectively along with TeOx peaks at 571.7 and 581.94 eV in Fig. 4b [53]. In the XPS spectrum of Ag 3d (Fig. 4c), the occurrence of two peaks at 367.8 and 373.8 eV corresponds to Ag $3d_{5/2}$ and Ag $3d_{3/2}$, respectively [54]. Meanwhile, in the core-level spectra of Mo 3d, the existence of Mo $3d_{5/2}$ and Mo $3d_{3/2}$ peaks at binding energies of 231.25 and 234.35 eV, respectively, as illustrated in Fig. 4d [54]. The spectrum of oxygen 1s (Fig. 4e) shows two peaks at 530.8 and 528.9 eV validating the metal oxide (AgMo–O) bond and O–H bond, respectively [46]. The survey spectrum of Ag_2MoO_4/Bi_2Te_3 nanocomposites is displayed in Fig. 4f.

3.2. Dispersion stability assessment of nanofluids

The long-lasting dispersion stability of the prepared nano additives is important and makes a substantial contribution to minimizing friction and wear. The dispersion stability of these nano additives in paraffin oil (PO) was achieved by diluting the optimized concentration up to 10 times using UV/visible spectroscopy (S2). The measurement of the absorbance value of the nano lubricants was recorded in the range of 300–700 nm wavelengths initiated from 0 to 96 h at fixed time intervals. The graphical representation of the changes in relative absorbance with settling time (h) is shown in Fig. S2a. A decline in relative absorbance over time is expected for all nano lubricants, however, this reduction is least pronounced for the Ag_2MoO_4/Bi_2Te_3 nanocomposites. It is evident that the highest degree of dispersion stability is manifested for the most efficacious additive Ag_2MoO_4/Bi_2Te_3, nevertheless, the other additives also have an adequate level of stability. The inset of Fig. S2a illustrates the absorbance of Ag_2MoO_4/Bi_2Te_3 nanocomposites for a duration extending from 0 to 96 h. Fig. S2b shows the images of PO and its blends with various nanoadditives captured initially and after 10 days.

3.3. Sample preparation and assessment of tribological characteristics

The characteristics of the PO utilized as a base oil are provided in the supporting information (S1.2) file in the present investigation. For optimizing the concentration of nano lubricants, 1-h ultra-sonication has been carried out at ambient temperature and a series of blends including as-synthesized nano additives in PO were prepared at 0.000, 0.015, 0.03, 0.06, and 0.09 %w/v. The antiwear characteristics for all combinations were executed on a Four-Ball Tester machine using ASTM D4172 test conditions. Additionally, load ramp assessments were conducted following the regulations of ASTM D5183 norms. The experimental details regarding the test procedures are depicted in S1., while their related tribological parameters are delineated in S1.3. The analysis of the worn surfaces after tribological tests was performed using AFM, SEM, and XPS techniques (S1.4).

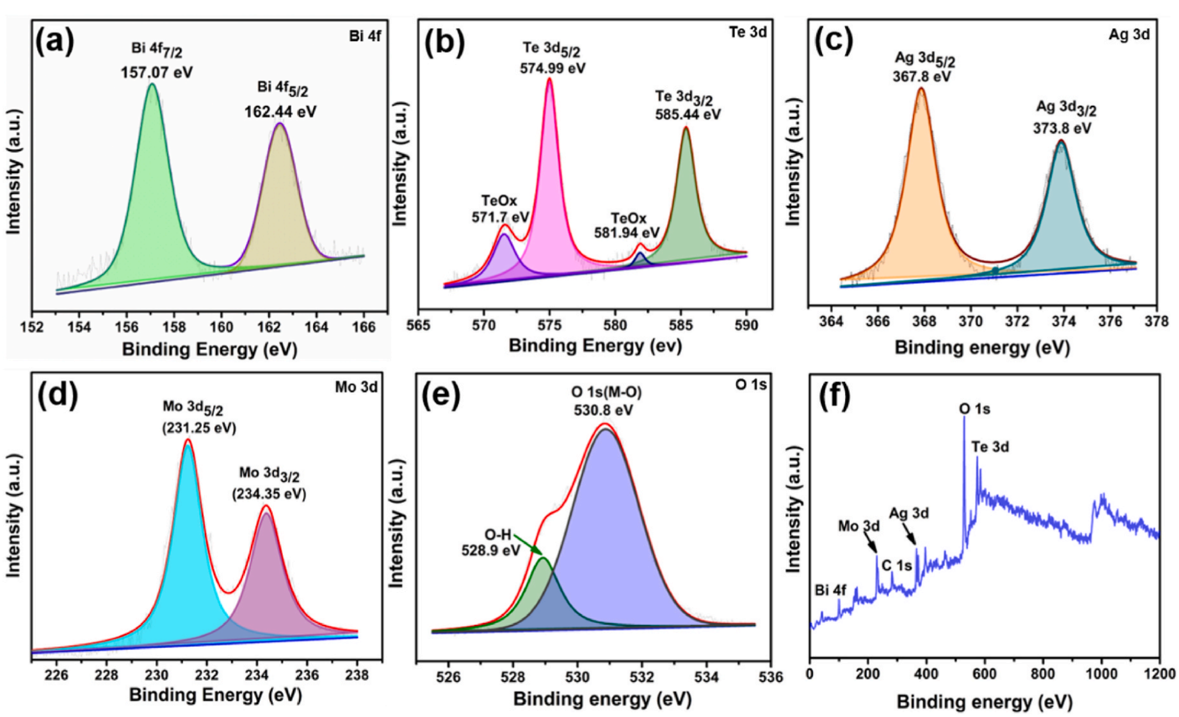

Fig. 4. XPS spectra of Ag_2MoO_4/Bi_2Te_3 nanocomposites (a) Bi 4f (b) Te 3d (c) Ag 3d (d) Mo 3d (e) O 1s and (f) survey spectrum of Ag_2MoO_4/Bi_2Te_3.

3.3.1. Analysis of optimal concentration of nano lubricants

Regarding the efficacy of nanoadditives, optimization of concentration is very important. The optimization process included an anti wear test using ASTM D4172 test norms (operating at 1200 rpm, applying a load of 392 N for 1 h) on blends of nano additives with varying concentrations (0.000, 0.015, 0.03, 0.06, and 0.09 % w/v) in PO. The corresponding mean wear scar diameter (MWD) values are depicted in Fig. 5a. A noticeable decrease in MWD values compared to the base lubricant was observed for all concentrations of the nano additives under investigation. However, all tested nano additives exhibited antiwear properties at each concentration, albeit with varying degrees of effectiveness. The MWD of pure paraffin oil was recorded as 0.735 mm. The higher value of MWD of base lube indicates that all additives exhibit superior antiwear characteristics compared to the base oil. The MWD values showed a decreasing trend from the plain PO to higher concentrations of 0.015 and 0.03 % w/v, with a subsequent increase for the upcoming concentrations, except for Ag_2MoO_4 (lowest MWD at 0.06 % w/v). Therefore, 0.03 % w/v was identified as the optimal concentration for tribological assessments of all the nano additives. The sequence of decreasing MWD values was as follows: Bi_2Te_3 (0.590 mm), Ag_2MoO_4 (0.500 mm), and Ag_2MoO_4/Bi_2Te_3 (0.355 mm). Thus, the Ag_2MoO_4/Bi_2Te_3 nanocomposites showed the most significant decrease in MWD compared to all other tested nano additives.

3.3.2. Antiwear and antifriction properties

The antiwear activity of blends containing all additives in paraffin oil (PO) was examined using the standard test ASTM D4172. The key parameters, MWD, and the average coefficient of friction (COF) were presented in a bar graph for all the nano additives (Fig. 5b).

The bar graph shows that MWD consistently decreased compared to pure PO (0.735 mm) in all the nano additives. The percentage reduction in MWD follows the sequence of Bi_2Te_3 (19.7 %), Ag_2MoO_4 (31.97 %), and Ag_2MoO_4/Bi_2Te_3 (51.7 %). In Fig. 5b, a significant drop in the average COF of PO (0.0756) was detected when the additives were present. The percentage reduction in average COF lies in the following order: Ag_2MoO_4 (24.823 %), Bi_2Te_3 (32.050 %), and Ag_2MoO_4/Bi_2Te_3 (47.578 %).

Fig. 5c displayed the variation of coefficient of friction with sliding time for both the PO and the blends incorporating nano additives at an optimized concentration of 0.03 % w/v on a 392 N load. Initially, there is a notably high COF for the base lubricant and its additive mixtures due to the absence of a tribo chemical film. As in situ tribofilm formation commences, the COF decreases and stabilizes upon the completion of the tribofilm. The remarkable efficacy of nano additives as friction and wear modifiers is evidenced by the smooth trajectory of the COF curve, contrasting with the erratic behavior observed in the case of PO. The characteristics of the tribofilm are reflected in the consistency of the COF curve. In the case of Ag_2MoO_4/Bi_2Te_3 nanocomposites, the interaction between Ag_2MoO_4 NPs and Bi_2Te_3 NSs results in the formation of an adhesive, uniform, and durable tribofilm which effectively minimizes the direct contact of matting surfaces and reduces the MWD and COF values remarkably.

3.3.3. Load-carrying ability

To study the load-carrying capability of prepared nanolubricants a standard ASTM D5183 test was utilized. This test was performed under specific conditions: a 392 N load, 600 rpm, 75 °C temperature, and for a 1-h period to complete the running-in period at the optimal additive concentration. Following this, a steady-state test was conducted by gradually adding a 98 N load every 10 min until a sudden increase in frictional torque value culminated in seizure load as illustrated in Fig. 5d. The graph displaying frictional torque versus time and load, clearly shows that at a 1078 N load, there is a sharp rise in frictional torque value for PO, resulting in the surface seizure. This particular load is identified as the seizure load, where the tribofilm stops to function, and the lubricant becomes inadequate to sustain the load. The presence of additives delays the failure, of tribofilm which occurs comparatively at a higher applied load. The enhancement in load-bearing capacity of the PO with admixtures was deduced from seizure loads: plain PO (1078 N), Bi_2Te_3 (1666 N), Ag_2MoO_4 (2450 N), and Ag_2MoO_4/Bi_2Te_3 (2646 N). Therefore, the superior load-carrying capacity is evident for the Ag_2MoO_4/Bi_2Te_3 nanocomposites.

3.3.4. Frictional power loss

The frictional power loss (P) calculations of the base oil in the presence and absence of nano additives have been done by utilizing

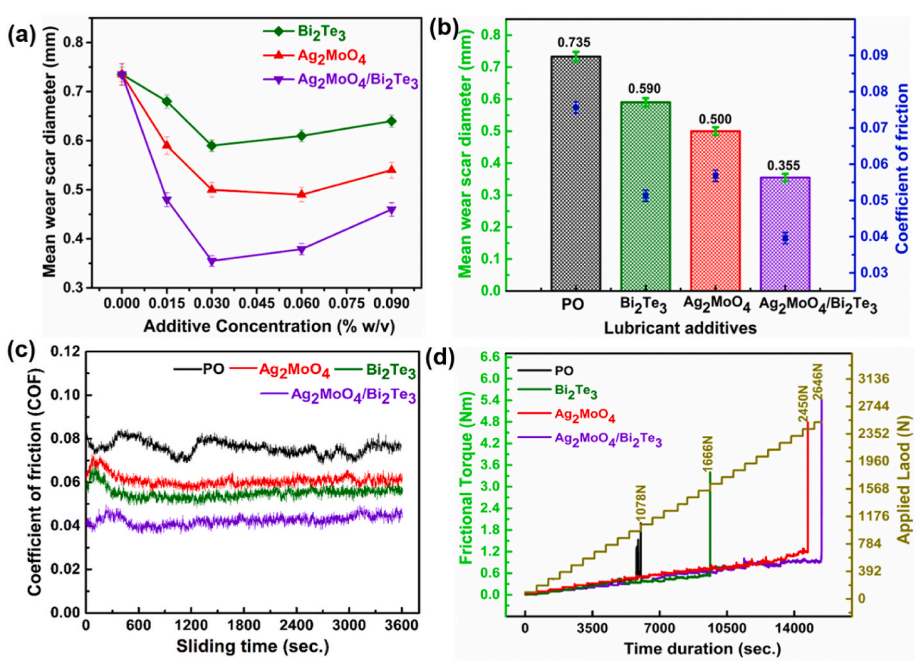

Fig. 5. (a) Optimization of additive concentration, (b) Represents average COF and MWD as a bar diagram, (c) illustrates COF over sliding duration, and (d) Compares frictional torque against load and time for plain PO and various additives following ASTM D5183 standards.

equation (1). The obtained results are provided in S1.3.3

$$P = 0.221 \times 3.6 \times \mu \, MJ \quad (1)$$

where μ represents the coefficient of friction,

Based on the data in Table S1, the base oil showed the highest power consumption at 0.0601 MJ. However, there was a significant reduction in power consumption for its mixtures with various nano additives, and a notable decrease in power consumption was observed: 0.0452 for Ag_2MoO_4, 0.0408 MJ for Bi_2Te_3, and 0.0315 MJ for the Ag_2MoO_4/Bi_2Te_3 nanocomposites. As a result, the Ag_2MoO_4/Bi_2Te_3 nanocomposite is associated with the lowest power consumption, leading to the highest level of energy conservation.

3.4. Morphological analysis of the wear scar surface

Surface analysis techniques such as SEM and AFM were employed to study the worn areas on steel balls exposed to nano additive blends after ASTM D4172 tests. Fig. 6(a–d) shows SEM images of the worn tracks lubricated with pure paraffin oil (PO) and its mixtures with various nano additives (0.03 % w/v).

The SEM micrograph of the base lubricant reveals a highly rough surface, with severe scratches. In contrast, the addition of nano additives significantly improved the smoothness of the worn surface enhancing the observed tribological properties of the nano additives. The MWD measurements in the inset images of Fig. 6(a–d), correlate well with surface uniformity. The MWD values show notable reductions; PO (0.735 mm), Bi_2Te_3 (0.590 mm), Ag_2MoO_4 (0.500 mm), and Ag_2MoO_4/Bi_2Te_3 (0.355 mm). A magnificent smooth surface is achieved through the use of blends containing Ag_2MoO_4/Bi_2Te_3 nanocomposites. The EDX (Fig. 6 e) and elemental mapping (Fig. S3) of the depleted surface lubricated with the Ag_2MoO_4/Bi_2Te_3 nanocomposites revealed the presence of all constituent elements; Bi, Te, Ag, Mo, and O, indicating their successful adsorption on the worn track.

The roughness of the lubricated surfaces of steel balls with and without nano additives during the ASTM D4172 test was examined using contact-mode AFM. The 3D AFM images of the worn scar surfaces are depicted in Fig. 7a-d, showing the surface roughness values for various mixtures, Sq and Rq, area roughness, and line roughness, respectively. A huge reduction in Rq (919-56 nm) and Sq (626-60 nm) values was observed on going from the plain PO to Ag_2MoO_4/Bi_2Te_3 nanocomposites. The utilization of the nanocomposites as an additive resulted in a remarkably smooth surface with minimal roughness, as depicted in Fig. 7d. Therefore, the AFM findings align well with the analysis of SEM results.

3.5. XPS analysis of the tribofilm

After the ASTM D4172 antiwear test, the XPS spectra of the wear track lubricated with Ag_2MoO_4/Bi_2Te_3 nanocomposites were examined to analyze the chemical states of elements present in the in situ formed tribofilm.

The deconvoluted core-level spectra of Ag 3d, Mo 3d, O 1s, Bi 4f, Te 3d, C 1s, and Fe 2p were presented in Fig. 8a-g using peak-fit software. Fig. 8a displays the XP spectrum of Ag 3d, wherein the Ag 3d $_{5/2}$ and 3d $_{3/2}$ peaks present at binding energies of 368.21 and 374.28 eV, respectively, due to the formation of Ag_2O [54,55,56]. The XPS graph of Mo 3d is represented in Fig. 8b and shows binding energies at 232.5 and 235.5 eV corresponding to Mo $3d_{5/2}$ and $3d_{3/2}$ respectively suggesting the formation of MoO_3, additionally one peak around 230.36 eV, is due to the MoO_2 formation [57]. In Fig. 8c, the spectra of O 1s is shown, which is almost similar to the O 1s spectra of the nanocomposite [46]. Fig. 8d represents the core-level spectra of Bi 4f showing peaks at 158.34 and 163.68 eV corresponding to Bi $4f_{7/2}$ and $4f_{5/2}$, respectively, validating the formation of Bi_2O_3 [58]. The formation of the Bi–O bond is plausibly ascribed to the oxidation of Bi_2Te_3 under the tribo-test conditions. XPS of Te 3d is shown in Fig. 8e, where the existence of Te $3d_{5/2}$ and $3d_{3/2}$ peaks at binding energies of 574.54 and 585.03 eV, respectively is ascribed due to the Bi–Te bond. In addition, two peaks around 572.26 and 587.89 eV are present due to the formation of tellurium oxides during the antiwear test [53,59]. Fig. 8f shows the XPS spectra of C 1s, originating from the carbon component of the base oil (paraffin oil), including binding energies at 284.1 and 287.4 eV, corresponding to C–C and C–O bonds, respectively [10]. The XPS investigation indicates that tribochemical oxidation results in the oxide formation of silver, molybdenum, bismuth, and tellurium. Additionally, the Fe 2p spectrum showed peaks at 711.14 and 724.68 eV for Fe $2p_{3/2}$ and Fe $2p_{1/2}$, respectively, with a peak around 719.33 eV, validating the Fe_2O_3 formation on the surface of the steel ball [10,28,51]. Thus, the assessment of the tribofilm through XPS suggests that tribofilm contains tribochemically oxidized metal oxides such as Ag_2O, MoO_3, MoO_2, Bi_2O_3,

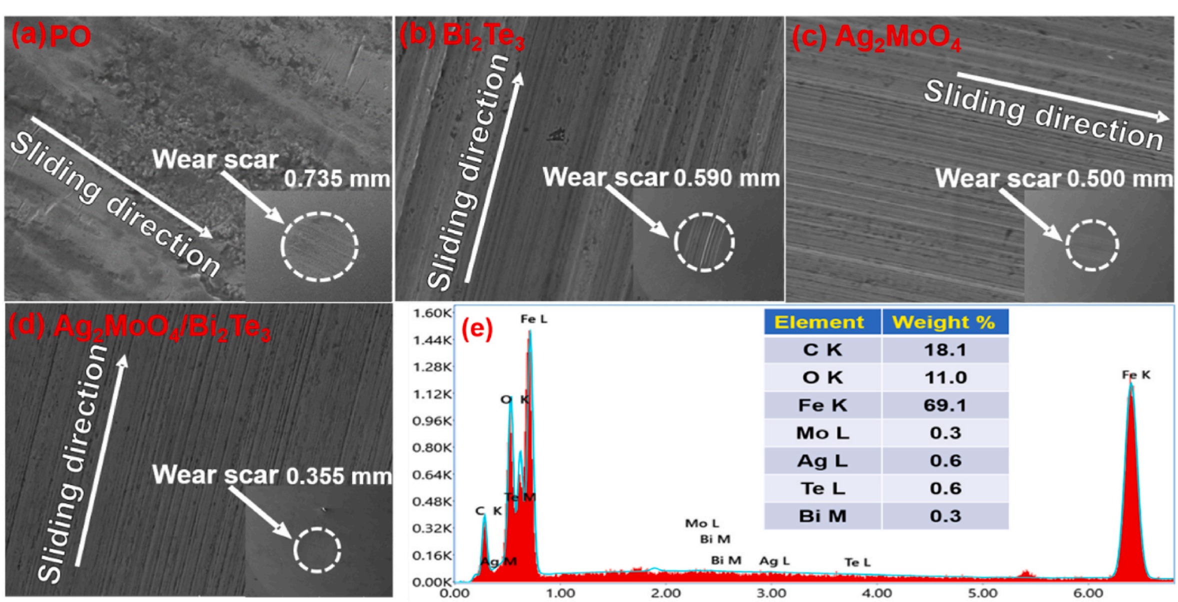

Fig. 6. (a–d) SEM images of lubricated surfaces of PO and with its admixtures (0.03 % w/v), at 2.00K × magnification with an inset of the wear scar at 100 × (e) EDX spectrum of the wear track lubricated with Ag_2MoO_4/Bi_2Te_3 nanocomposites.

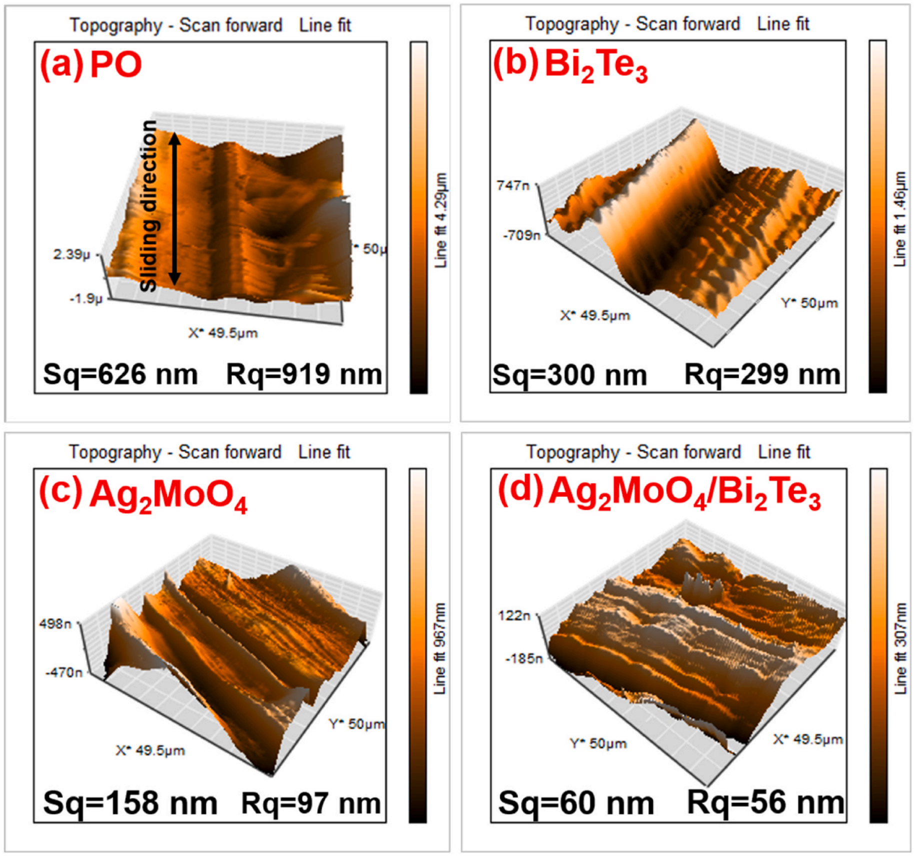

Fig. 7. 3D AFM images of the wear track with PO and its blends at the optimal concentration (0.03 % w/v): (a) PO, (b) Bi_2Te_3, (c) Ag_2MoO_4, and (d) Ag_2MoO_4/Bi_2Te_3 nanocomposites.

TeO_2, Fe_2O_3, etc., which collectively contribute to significant improvement in the tribological activity of nanocomposites.

3.6. Plausible lubrication mechanism

The in situ formed tribofilm on the lubricated surface during the antiwear test plays a crucial role in comparing the lubrication performance of different nano lubricants. At first, there is no tribofilm on the worn surface, and the nano additives just stick to the surfaces physically. Later on, chemical interactions start, leading to the formation of tribofilm under tribo-stress conditions. The movement of Bi_2Te_3 nanosheets over each other is facilitated by the presence of weak van der Waals forces between them, leading to their intrinsic lubricity. The incorporation of nanoparticles between the nanosheets of Bi_2Te_3 prevents the clustering of nanosheets. The sliding motion is expedited by the layered structure of Bi_2Te_3, and the reinforcement of Ag_2MoO_4 nanoparticles in between the Bi_2Te_3 nanosheets functions as spacers, thus alleviating the re-stacking phenomenon. Additionally, the nanoparticles strengthened the nanosheets and hindered their clustering, thereby improving their dispersion in the base lubricant. Conversely, a simultaneous decrease in the agglomeration of nanoparticles was observed due to the presence of nanosheets. These nanoparticles work as nano-bearings, positioned between the nanosheets and the nearby surfaces, thereby reducing friction and wear. Nanoparticles fill the asperities on the contact surfaces, and nanosheets form a protective layer, preventing direct contact between the surfaces. Their synergistic effect can lead to improved load-carrying capacity, reduced friction, and enhanced wear resistance. As a result, the sliding movement was further facilitated, leading to an enhancement in lubrication. Furthermore, the nanoparticles contributed to improving the lubrication by undergoing tribo-sinterization on the contacting surfaces. The outstanding tribological performance of the nanocomposites is elucidated through a proposed mechanistic diagram displayed in Fig. 9.

The XPS analysis of the tribochemical film developed on the depleted surface lubricated with blends of Ag_2MoO_4/Bi_2Te_3 nanocomposites during the ASTM D4172 test demonstrates the presence of various metal oxides, including Bi_2O_3, TeO_2, Ag_2O, MoO_3, MoO_2, and Fe_2O_3. The interaction between these components has produced a synergistic outcome resulting in a notable enhancement in the tribological behavior of nanocomposites.

4. Conclusions

The hydrothermal, and co-precipitation methods were used to synthesize Bi_2Te_3 nanosheets, and Ag_2MoO_4 nanoparticles, respectively. The Ag_2MoO_4/Bi_2Te_3 nanocomposites were prepared employing an in situ co-precipitation strategy. Various state-of-the-art techniques (HR-SEM with EDX, TEM, HR-TEM, FT-IR, and p-XRD) were used to characterize the synthesized nano additives. Additionally, the XPS analysis has been utilized to investigate the chemical states of elements present in Ag_2MoO_4/Bi_2Te_3 nanocomposites. The structure of the nanocomposites shows that the nanoparticles are decorated onto the nanosheets and are attached by weak physical interactions. The nano additives stayed stable in paraffin oil for 96 h, as shown by absorbance measurements using UV/visible spectroscopy. Evaluation of the antiwear and antifriction performance of the synthesized nanomaterials using the ASTM D4172 norms, and load-bearing capability (ASTM D5183) test at an optimized concentration of 0.03 %w/v on a four-ball tester machine reveals the superior tribological properties of Ag_2MoO_4/Bi_2Te_3 nanocomposites. The SEM and AFM investigations of the wear pathway corroborate the result of antiwear and antifriction. XPS analyses of the wear track reveal that the tribofilm comprises Ag_2MoO_4, adsorbed Bi_2Te_3, and Fe_2O_3. The

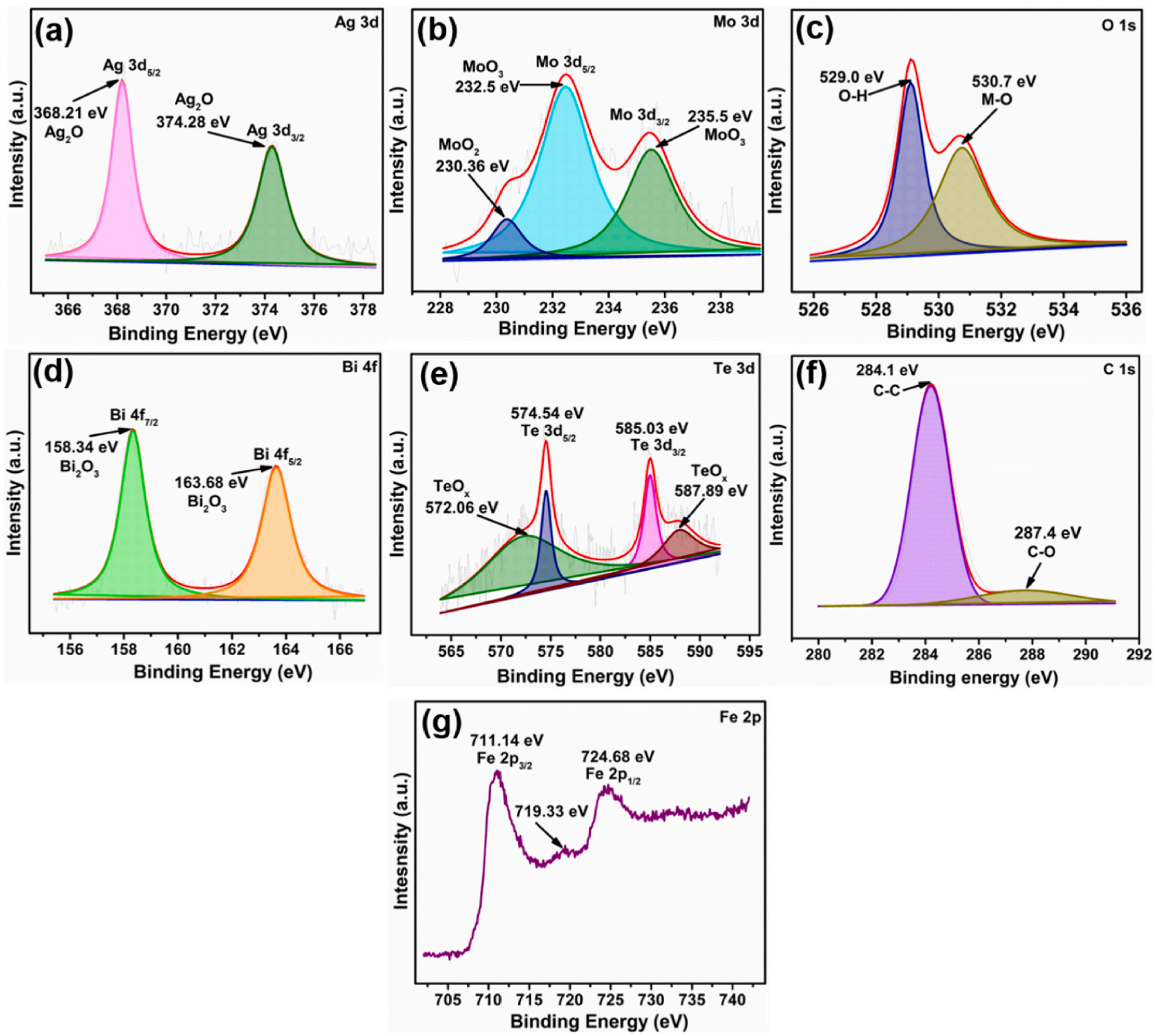

Fig. 8. Deconvoluted XPS of the in situ formed tribofilm on the wear track surface lubricated with blends of Ag_2MoO_4/Bi_2Te_3 nanocomposites: (a) Ag 3d, (b) Mo 3d, (c) O 1s, (d) Bi 4f, (e) Te 3d, (f) C 1s and (g) Fe 2p.

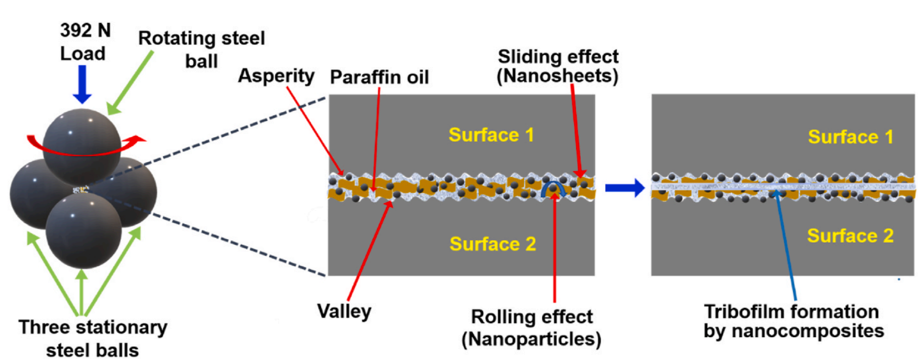

Fig. 9. Schematic diagram of the plausible lubrication mechanism.

combined influence of tribosinterization and rolling mechanisms augmented the lubrication performance of the nanoparticles. The nanoparticles served as spacers between the nanosheets, thereby regulating their stacking configuration. The excellent triboactivity of the Ag_2MoO_4/Bi_2Te_3 nanocomposites can be attributed to the synergistic interactions between the nanoparticles and nanosheets. The proposed nanocomposite may have great potential as an efficient antiwear and antifriction agent for tribological applications.

CRediT authorship contribution statement

Somesh Singh: Writing – original draft, Methodology, Investigation. **Muskan Sahu:** Formal analysis, Data curation. **Satypal Prajapati:** Formal analysis, Data curation. **Anup Kumar:** Formal analysis. **Murli Dhar Mitra:** Writing – review & editing, Formal analysis, Data curation. **Aditya Kumar:** Writing – review & editing. **Dhanesh Tiwary:** Writing – review & editing, Resources. **Dinesh K. Verma:** Writing – review &

editing, Validation, Supervision, Project administration, Funding acquisition.

Notes

The authors have declared no competing financial interests.

Declaration of competing interest

The authors declare the following financial interests/personal relationships which may be considered as potential competing interests: Dr. Dinesh Kumar Verma reports financial support was provided by State Council of Science and Technology Uttar Pradesh. Dr. Dinesh Kumar Verma reports financial support was provided by Higher Education Department Uttar Pradesh. If there are other authors, they declare that they have no known competing financial interests or personal relationships that could have appeared to influence the work reported in this paper.

Acknowledgements

The author, Dinesh K. Verma would like to express gratitude to the Council of Science & Technology, U.P. (Letter No. CST/CHEM/D-1112, dt. August 25, 2022), and Centre of Excellence (78/2024/1015/सत्तर-4-2024-001-70-4002(002)/4/2023) for providing financial support. All the contributing authors of this manuscript give their profound gratitude to the CIFC Incharge, IIT-BHU, Varanasi, India, for availing XRD, FT-IR, SEM/EDX, and CRF Incharge IIT-ISM, Dhanbad, India, for XPS, and TEM, facilities.

Appendix A. Supplementary data

Supplementary data to this article can be found online at https://doi.org/10.1016/j.hybadv.2025.100429.

References

[1] A. Rosenkranz, M.C. Righi, A.V. Sumant, B. Anasori, V.N. Mochalin, Perspectives of 2D MXene tribology, Adv. Mater. 35 (2023) 2207757, https://doi.org/10.1002/adma.202207757.
[2] Deepika, Nanotechnology implications for high performance lubricants, SN Appl. Sci. 2 (2020) 1128, https://doi.org/10.1007/s42452-020-2916-8.
[3] V. Cortes, K. Sanchez, R. Gonzalez, M. Alcoutlabi, J.A. Ortega, The performance of SiO2 and TiO2 nanoparticles as lubricant additives in sunflower oil, Lubricants 8 (2020) 10, https://doi.org/10.3390/lubricants8010010.
[4] B. Wang, F. Qiu, G.C. Barber, Q. Zou, J. Wang, S. Guo, Y. Yuan, Q. Jiang, Role of nano-sized materials as lubricant additives in friction and wear reduction: a review, Wear 490–491 (2022) 204206, https://doi.org/10.1016/j.wear.2021.204206.
[5] A.V. Bondarev, A. Fraile, T. Polcar, D.V. Shtansky, Mechanisms of friction and wear reduction by *h*-BN nanosheet and spherical W nanoparticle additives to base oil: experimental study and molecular dynamics simulation, Tribol. Int. 151 (2020) 106493, https://doi.org/10.1016/j.triboint.2020.106493.
[6] N. Shukla, D.K. Verma, A.K. Singh, B. Kumar, Kavita, R.B. Rastogi, Ternary composite of methionine-functionalized graphene oxide, lanthanum-doped yttria nanoparticles, and molybdenum disulfide nanosheets for thin-film lubrication, ACS Appl. Nano Mater. 3 (2020) 8012–8026, https://doi.org/10.1021/acsanm.0c01468.
[7] A.D. Thampi, M.A. Prasanth, A.P. Anandu, E. Sneha, B. Sasidharan, S. Rani, The effect of nanoparticle additives on the tribological properties of various lubricating oils – review, Mater. Today Proc. 47 (2021) 4919–4924, https://doi.org/10.1016/j.matpr.2021.03.664.
[8] M. Waqas, R. Zahid, M.U. Bhutta, Z.A. Khan, A. Saeed, A review of friction performance of lubricants with nano additives, Materials 14 (2021) 6310, https://doi.org/10.3390/ma14216310.
[9] B. Kumar, D.K. Verma, Kavita, R.B. Rastogi, Tribological activity of ionic liquid stabilized calcium-doped ceria nanoparticles, Proc. Inst. Mech. Eng. Part J J. Eng. Tribol. 235 (2021) 989–996, https://doi.org/10.1177/1350650120935005.
[10] D.K. Verma, S. Prajapati, M. Sahu, S. Singh, B. Kumar, A.K. Singh, N. Shukla, Kavita, R.B. Rastogi, Superlubricity of nanocomposites of polyaniline-functionalized reduced graphene oxide with yttrium and vanadium-codoped zinc oxide nanoparticles, ACS Appl. Eng. Mater. 2 (2024) 156–169, https://doi.org/10.1021/acsaenm.3c00683.
[11] Kavita, A.K. Singh, N. Shukla, B. Kumar, D.K. Verma, J.L. Maurya, S. Singh, R. B. Rastogi, Improvement of tribo-active behavior of g-C3N4 nanosheets using m-LaVO4 nanoparticles, Colloids Surf. A Physicochem. Eng. Asp. 663 (2023) 131031, https://doi.org/10.1016/j.colsurfa.2023.131031.
[12] B. Xin, Y. Yu, J. Zhou, L. Wang, S. Ren, Effect of copper molybdate on the lubricating properties of NiCrAlY laser clad coating at elevated temperatures, Surf. Coat. Technol. 313 (2017) 328–336, https://doi.org/10.1016/j.surfcoat.2017.01.098.
[13] J. Yang, J. Jia, X. Li, C. Lu, X. Feng, Synergistic lubrication of Ag and Ag2MoO4 nanoparticles anchored in plasma-sprayed YSZ coatings: remarkably-durable lubricating performance at 800 °C, Tribol. Int. 153 (2021) 106670, https://doi.org/10.1016/j.triboint.2020.106670.
[14] E. Hao, Y. An, J. Chen, X. Zhao, G. Hou, J. Chen, M. Gao, F. Yan, In-situ formation of layer-like Ag2MoO4 induced by high-temperature oxidation and its effect on the self-lubricating properties of NiCoCrAlYTa/Ag/Mo coatings, J. Mater. Sci. Technol. 75 (2021) 164–173, https://doi.org/10.1016/j.jmst.2020.10.024.
[15] W. Zhu, A.R. Kamali, Green preparation of nanostructured β-MoO3/hexagonal-shaped MoS2/graphene with enhanced lithium-ion storage performance, J. Alloys Compd. 932 (2023) 167724, https://doi.org/10.1016/j.jallcom.2022.167724.
[16] E.L. Castellanos-Leal, A. Osuna-Zatarain, A. Garcia-Garcia, Frictional properties of two-dimensional nanomaterials as an additive in liquid lubricants: current challenges and potential research topics, Lubricants 11 (2023) 137, https://doi.org/10.3390/lubricants11030137.
[17] X. Zhang, T. Ren, Z. Li, Recent advances of two-dimensional lubricating materials: from tunable tribological properties to applications, J. Mater. Chem. A 11 (2023) 9239–9269, https://doi.org/10.1039/D2TA08489A.
[18] W. Zhao, X. Ci, TiO2 nanoparticle/fluorinated reduced graphene oxide nanosheet composites for lubrication and wear resistance, ACS Appl. Nano Mater. 3 (2020) 8732–8741, https://doi.org/10.1021/acsanm.0c01547.
[19] R. Wang, F. Zhang, K. Yang, Y. Xiong, J. Tang, H. Chen, M. Duan, Z. Li, H. Zhang, B. Xiong, Review of two-dimensional nanomaterials in tribology: recent developments, challenges and prospects, Adv. Colloid Interface Sci. 321 (2023) 103004, https://doi.org/10.1016/j.cis.2023.103004.
[20] K.N. Sidh, D. Jangra, H. Hirani, An experimental investigation of the tribological performance and dispersibility of 2D nanoparticles as oil additives, Lubricants 11 (2023) 179, https://doi.org/10.3390/lubricants11040179.
[21] A. Dhanola, K.K. Gajrani, Novel insights into graphene-based sustainable liquid lubricant additives: a comprehensive review, J. Mol. Liq. 386 (2023) 122523, https://doi.org/10.1016/j.molliq.2023.122523.
[22] Q. Wang, J. Du, R. Ouyang, B. Liu, Y. Miao, Y. Li, Recent advances in functional bismuth chalcogenide nanomaterials: cancer theranostics, antibacterial and biosensing, Coord. Chem. Rev. 492 (2023) 215281, https://doi.org/10.1016/j.ccr.2023.215281.
[23] J. Ni, X. Bi, Y. Jiang, L. Li, J. Lu, Bismuth chalcogenide compounds Bi2×3 (X=O, S, Se): applications in electrochemical energy storage, Nano Energy 34 (2017) 356–366, https://doi.org/10.1016/j.nanoen.2017.02.041.
[24] C. Müller, F.L. Redondo, M. Dennehy, A.E. Ciolino, W.R. Tuckart, Bismuth (III) sulfide as additive: towards better lubricity without toxicity, Ind. Lubric. Tribol. 70 (2018) 347–352, https://doi.org/10.1108/ILT-03-2017-0051.
[25] R.T. Hart, A.A. Kerr, N.A. Eckert, Bismuth sulfide (Bi2S3) as the active species in extreme pressure lubricants containing bismuth carboxylates and sulfur compounds, Tribol. Trans. 53 (2009) 22–28, https://doi.org/10.1080/10402000903154816.
[26] P. Gonzalez-Rodriguez, K.J.H. van den Nieuwenhuijzen, W. Lette, D.J. Schipper, J. E. ten Elshof, Tribochemistry of bismuth and bismuth salts for solid lubrication, ACS Appl. Mater. Interfaces 8 (2016) 7601–7606, https://doi.org/10.1021/acsami.6b02541.
[27] B. Pilotti, G. Prieto, A. Juan, R. Faccio, E. Broitman, M. Dennehy, W.R. Tuckart, Bi2S3 and MoS2 soft coatings: a comparative study of their frictional behavior under different humidity levels, normal loads, and sliding speeds, Tribol. Lett. 69 (2021) 112, https://doi.org/10.1007/s11249-021-01486-y.
[28] N. Shukla, A.K. Singh, Kavita, D.K. Verma, B. Kumar, J.L. Maurya, D. Tiwary, R. B. Rastogi, Heterolamellar Bi2Se3/Bi2WO6 and Bi2Se3/N-doped Bi2WO6 nanosheet composites as potential antifriction and antiwear agents, ACS Appl. Eng. Mater. 1 (2023) 1322–1334, https://doi.org/10.1021/acsaenm.3c00039.
[29] D. Wu, J. Guo, Z.-H. Ge, J. Feng, Facile synthesis Bi2Te3 based nanocomposites: strategies for enhancing charge carrier separation to improve photocatalytic activity, Nanomaterials 11 (2021) 3390, https://doi.org/10.3390/nano11123390.
[30] T.Q. Kimberly, K.M. Ciesielski, X. Qi, E.S. Toberer, S.M. Kauzlarich, High thermoelectric performance in 2D Sb2Te3 and Bi2Te3 nanoplate composites enabled by energy carrier filtering and low thermal conductivity, ACS Appl. Electron. Mater. (2023), https://doi.org/10.1021/acsaelm.3c00385.
[31] X. Chen, L. Feng, P. Yu, C. Liu, J. Lan, Y.-H. Lin, X. Yang, Flexible thermoelectric films based on Bi2Te3 nanosheets and carbon nanotube network with high n-type performance, ACS Appl. Mater. Interfaces 13 (2021) 5451–5459, https://doi.org/10.1021/acsami.0c21396.
[32] M. Tang, J.-Y. Zhang, S. Bi, Z.-L. Hou, X.-H. Shao, K.-T. Zhan, M.-S. Cao, Ultrathin topological insulator absorber: unique dielectric behavior of Bi2Te3 nanosheets based on conducting surface states, ACS Appl. Mater. Interfaces 11 (2019) 33285–33291, https://doi.org/10.1021/acsami.9b13775.
[33] C. Lu, M. Luo, W. Dong, Y. Ge, T. Han, Y. Liu, X. Xue, N. Ma, Y. Huang, Y. Zhou, X. Xu, Bi2Te3/Bi2Se3/Bi2S3 cascade heterostructure for fast-response and high-photoresponsivity photodetector and high-efficiency water splitting with a small bias voltage, Adv. Sci. 10 (2023) 2205460, https://doi.org/10.1002/advs.202205460.
[34] J.L. Liu, H. Wang, X. Li, H. Chen, Z.K. Zhang, W.W. Pan, G.Q. Luo, C.L. Yuan, Y. L. Ren, W. Lei, High performance visible photodetectors based on thin two-

dimensional Bi2Te3 nanoplates, J. Alloys Compd. 798 (2019) 656–664, https://doi.org/10.1016/j.jallcom.2019.05.299.
[35] F. Zhao, S. Zhou, Y. Zhang, Ultrasensitive detection of hydrogen peroxide using Bi2Te3 electrochemical sensors, ACS Appl. Mater. Interfaces 13 (2021) 4761–4767, https://doi.org/10.1021/acsami.0c19911.
[36] J. Liu, L. Ren, J. Luo, N. Lv, Hybrid Bi2Te3/Bi2TeO5 nanoscale flakes via chemical disproportionation under microwave: electrochemical supercapacitor applications, Ceram. Int. (2024), https://doi.org/10.1016/j.ceramint.2024.02.324.
[37] A. Nour, R.S. Hamida, A. El-Dissouky, H.M.A. Soliman, H.M. Refaat, One-pot facile synthesis of hexagonal Bi2Te3 nanosheets and its novel nanocomposites: characterization, anticancer, antibacterial, and antioxidant activities, Colloids Surf. B Biointerfaces 225 (2023) 113230, https://doi.org/10.1016/j.colsurfb.2023.113230.
[38] S. Wang, Y. Qiao, X. Liu, S. Zhu, Y. Zheng, H. Jiang, Y. Zhang, J. Shen, Z. Li, Y. Liang, Z. Cui, P.K. Chu, S. Wu, Reduced graphene oxides modified Bi2Te3 nanosheets for rapid photo-thermoelectric catalytic therapy of bacteria-infected wounds, Adv. Funct. Mater. 33 (2023) 2210098, https://doi.org/10.1002/adfm.202210098.
[39] J.M. Liñeira del Río, F. Mariño, E.R. López, D.E.P. Gonçalves, J.H.O. Seabra, J. Fernández, Tribological enhancement of potential electric vehicle lubricants using coated TiO2 nanoparticles as additives, J. Mol. Liq. 371 (2023) 121097, https://doi.org/10.1016/j.molliq.2022.121097.
[40] Chemically modified nanomaterials as lubricant additive: time stability, friction, and wear, J. Mol. Liq. 382 (2023) 121913, https://doi.org/10.1016/j.molliq.2023.121913.
[41] D.K. Verma, B. Kumar, Kavita, R.B. Rastogi, Zinc oxide- and magnesium-doped zinc oxide-decorated nanocomposites of reduced graphene oxide as friction and wear modifiers, ACS Appl. Mater. Interfaces 11 (2019) 2418–2430, https://doi.org/10.1021/acsami.8b20103.
[42] D.K. Verma, N. Shukla, B. Kumar, A.K. Singh, K. Shahu, M. Yadav, K.Y. Rhee, R. B. Rastogi, Synergistic tribo-activity of nanohybrids of zirconia/cerium-doped zirconia nanoparticles with nano lamellar reduced graphene oxide and molybdenum disulfide, Nanomaterials 10 (2020) 707, https://doi.org/10.3390/nano10040707.
[43] A.K. Singh, N. Shukla, D.K. Verma, Kavita, B. Kumar, R.B. Rastogi, Enhancement of triboactivity of nanolamellar graphitic-C3N4 by N-doped ZnO nanorods, Ind. Eng. Chem. Res. 60 (2021) 864–874, https://doi.org/10.1021/acs.iecr.0c03955.
[44] R. Kumar, M. Antonov, M. Varga, I. Hussainova, M. Rodriguez Ripoll, Synergistic effect of Ag and MoS2 on high-temperature tribology of self-lubricating NiCrBSi composite coatings by laser metal deposition, Wear (2023) 532–533, https://doi.org/10.1016/j.wear.2023.205114, 205114.
[45] Z. Zhang, X. Fan, X. Ma, M. Zhu, Synergistic lubrication mechanism of core/shell C@MoS2 particles as lubricant additives, Appl. Surf. Sci. 639 (2023) 158234, https://doi.org/10.1016/j.apsusc.2023.158234.
[46] N. Pachauri, G.B.V.S. Lakshmi, S. Sri, P.K. Gupta, P.R. Solanki, Silver molybdate nanoparticles based immunosensor for the non-invasive detection of Interleukin-8 biomarker, Mater. Sci. Eng. C 113 (2020) 110911, https://doi.org/10.1016/j.msec.2020.110911.
[47] S. Kokilavani, A.A. Al-Kheraif, A.M. Thomas, A. Syed, A.M. Elgorban, L.L. Raju, A. Das, S.S. Khan, Novel NiS/Ag2MoO4 heterostructure nanocomposite: synthesis, characterization and superior antibacterial and enhanced photocatalytic activity, Phys. E Low-Dimens. Syst. Nanostructures 133 (2021) 114767, https://doi.org/10.1016/j.physe.2021.114767.
[48] D.G. Della Rocca, M. Schneider, F.C. Fraga, A. De Noni Júnior, R.A. Peralta, E. Rodríguez-Aguado, E. Rodríguez-Castellón, R.F.P.M. Moreira, A comprehensive insight into the parameters that influence the synthesis of Ag2MoO4 semiconductors via experimental design, J. Mater. Sci. Mater. Electron. 34 (2023) 1500, https://doi.org/10.1007/s10854-023-10897-7.
[49] Y. Saberi, S.A. Sajjadi, H. Mansouri, Comparison of characteristics of Bi2Te3 and Bi2Te2.7Se0.3 thermoelectric materials synthesized by hydrothermal process, J. Mater. Sci. Mater. Electron. 31 (2020) 18988–18995, https://doi.org/10.1007/s10854-020-04435-y.
[50] M. Wu, H. Lv, T. Wang, Z. Ao, H. Sun, C. Wang, T. An, S. Wang, Ag2MoO4 nanoparticles encapsulated in g-C3N4 for sunlight photodegradation of pollutants, Catal. Today 315 (2018) 205–212, https://doi.org/10.1016/j.cattod.2018.01.019.
[51] A.K. Singh, N. Shukla, D.K. Verma, Kavita, B. Kumar, R.B. Rastogi, Enhancement of triboactivity of nanolamellar graphitic-C3N4 by N-doped ZnO nanorods, Ind. Eng. Chem. Res. 60 (2021) 864–874, https://doi.org/10.1021/acs.iecr.0c03955.
[52] B. Trawiński, B. Bochentyn, M. Łapiński, B. Kusz, A study of the kinetics of bismuth telluride synthesis by an oxide reduction method, Thermochim. Acta 683 (2020) 178437, https://doi.org/10.1016/j.tca.2019.178437.
[53] H. Shen, B. Jang, J. Park, H. Mun, H.-B. Cho, Y.-H. Choa, In situ synthesis of a Bi2Te3-nanosheet/reduced-graphene-oxide nanocomposite for non-enzymatic electrochemical dopamine sensing, Nanomaterials 12 (2022) 2009, https://doi.org/10.3390/nano12122009.
[54] R. Shejini, K. Mohanraj, J. Henry, G. Sivakumar, R. Akash, V. Sivashankar, Enhanced specific capacitance of Ni foam coated Ag2MoO4 symmetric supercapacitor synthesized by hydrothermal method, J. Mater. Sci. Mater. Electron. 35 (2024) 668, https://doi.org/10.1007/s10854-024-12420-y.
[55] Z. He, J. Su, R. Chen, B. Tang, Fabrication of novel p-Ag2O/n-PbBiO2Br heterojunction photocatalysts with enhanced photocatalytic performance under visible-light irradiation, J. Mater. Sci. Mater. Electron. 30 (2019) 20870–20880, https://doi.org/10.1007/s10854-019-02454-y.
[56] C. Shan, Z. Su, Z. Liu, R. Xu, J. Wen, G. Hu, T. Tang, Z. Fang, L. Jiang, M. Li, One-step synthesis of Ag2O/Fe3O4 magnetic photocatalyst for efficient organic pollutant removal via wide-spectral-response photocatalysis–fenton coupling, Molecules 28 (2023) 4155, https://doi.org/10.3390/molecules28104155.
[57] J. Wang, Z. Jiang, G. Peng, E. Hoenig, G. Yan, M. Wang, Y. Liu, X. Du, C. Liu, Surface valence state effect of MoO2+ on electrochemical nitrogen reduction, Adv. Sci. 9 (2022) 2104857, https://doi.org/10.1002/advs.202104857.
[58] G. Liu, S. Li, Y. Lu, J. Zhang, Z. Feng, C. Li, Controllable synthesis of α-Bi2O3 and γ-Bi2O3 with high photocatalytic activity by α-Bi2O3→γ-Bi2O3→α-Bi2O3 transformation in a facile precipitation method, J. Alloys Compd. 689 (2016) 787–799, https://doi.org/10.1016/j.jallcom.2016.08.047.
[59] B. Chen, H. Sahin, A. Suslu, L. Ding, M.I. Bertoni, F.M. Peeters, S. Tongay, Environmental changes in MoTe2 excitonic dynamics by defects-activated molecular interaction, ACS Nano 9 (2015) 5326–5332, https://doi.org/10.1021/acsnano.5b00985.